SPACE TELESCOPE SCIENCE INSTITUTE
Operated for NASA by AURA

Instrument Science Report ACS 2008-03

HST Focus Variations with Temperature

Daiana Di Nino, Russell B. Makidon, Matt Lallo, Kailash C. Sahu
Marco Sirianni, Stefano Casertano

May 7, 2008

Abstract

One of the main advantages of space observatories is the quality and stability of the point spread function that allows programs not feasible from the ground. However, when pushed to the limits, even the Hubble Space Telescope exhibits variations in the PSF that can be problematic for studies like weak lensing or identification of the host halos of bright quasars at high redshift. These variations are primarily due to small displacements in the focus of the telescope, which to a first approximation can be ascribed to temperature variations. The aim of this report is to characterize the variation of the focus position for HST in terms of the average temperature sensor values of the telescope. We propose a comprehensive temperature-focus model able to predict the position of the focus at the micron level over a dynamic range that extends from sub-orbital variations (< 1 hour) to seasonal and yearly variations. This allows us to predict the focus position significantly more accurately than using interpolation of the monthly direct measurements. Our model is also at least as accurate as the previously proposed breathing model for sub-orbital variations and it is the first one that describes longer term variations, potentially helping the determination of the model point spread function for observations lacking reference point sources.

Copyright © 2008 The Association of Universities for Research in Astronomy, Inc. All Rights Reserved.

Introduction

Mechanical dilations/contractions of the Hubble Space Telescope (HST), happening on many different timescales ranging from hours to years, affect the focus position of the telescope and the shape of the Point Spread Function (PSF).

An accurate knowledge of the PSF is fundamental to enhance the science value of many HST observations, such as identifications of the host halos of bright quasars at high redshift (e.g., Martel et al. 2003; Hamilton et al. 2008), weak lensing (e.g., Park et al. 2004; Rhodes et al. 2000), or separations of individual stars in close, binary systems (e.g., Ciardullo et al. 1999; Remage Evans et al. 2007). Other studies which will benefit from accurate knowledge of the PSF include accurate stellar photometry in crowded fields (e.g., Sahu et al. 2006), high-precision astrometry (e.g., Anderson & King 2003), study of debris disks around young stars (Schneider et al. 2006) and study of AGNs (e.g., McNeil et al. 2005). In fact not every observation has a sufficient number of bright stars in its field of view to measure directly the PSF, therefore the knowledge of the focus position would help to construct an accurate model using tools such as Tiny Tim (Krist & Hook 2004).

Unfortunately a direct focus measurement is not always readily feasible, as this requires the analysis of an appropriate dataset consisting of a field of bright stars. Therefore in the past there have been several attempts to characterize both the timescale for the focus variation and its relation with the measured temperatures. As summarized in Lallo et al. (2005), four main trends have been identified: (i) desorption shrinking, first quantified by Hasan (1993) as exponentially decreasing on a yearly timescale related to the loss of gas molecules trapped in the HST materials, which were previously at equilibrium at Earth pressure; (ii) seasonal oscillations related to the orbital precession of HST as well as to the Earth-Sun orbit (Suchkov 1998); (iii) wandering on a daily timescale related to the sun/telescope angle and therefore to the temperature of the telescope (Hershey 1997); (iv) hourly variations, called 'breathing', related to the orbital position of the telescope (Bély 1993).

Excluding the overall shrinkage due to desorption of gas molecules, most of the mechanical stresses on the telescope can be ascribed to a first approximation to temperature fluctuations, for which high frequency measurements are available. However, except for the short term breathing of the telescope, a comprehensive focus-temperature relation is missing. Recently, Sahu et al. (2007) carried out a preliminary investigation to construct this relation, finding a promising correlation between the temperature and the width of the PSF. Here we aim at providing an accurate and reliable model to describe the HST focus-temperature relation based on an extensive dataset of ACS/WFC measurements.

Input Data

Engineering Data

The thermal condition of the telescope is monitored every 5 minutes through hundreds of temperature sensors distributed throughout the whole spacecraft structure. So it is possible to define many different average temperatures just by considering different sensors or different functions of the sensor values. In 1997 Hershey identified 6 principal functions of the sensor readouts by selecting those that have a time dependence related to the orbital phase or to the telescope attitude. In this study, we use the same temperature definitions as they are now routinely calculated from the engineering telemetry.

In order to better understand these temperature definitions (see also Appendix C), let us subdivide the spacecraft structure into the following main sections (see Fig. 1):

1. The Light Shield, i.e., the forward (cylindrical) portion of the spacecraft that goes from the plane of the aperture door to the one of the secondary mirror (SM). For this section we consider 8 temperature sensors located on two rings about 40 inches from the edges of the light shield.

2. The Forward Shell, i.e., the central (cylindrical) portion of the spacecraft that goes from the plane of the secondary mirror to the Support System Module (SSM) and thus containing most of the Optical Telescope Assembly (OTA). For this section, we consider 8 temperature sensors located on two rings about 40 inches from the edges of the forward shell. This section contains also most of the cylindrical Metering Truss Structure (MTS) that holds the primary and the secondary mirrors, thus extending through the SSM section. We consider 12 temperature sensors located along the metering truss structure.

3. The Aft Shroud, i.e., the backward (cylindrical) portion of the spacecraft that goes from the SSM to the end of the spacecraft, thus containing the primary mirror and the Scientific Instruments (SI). For this section we consider 14 internal temperature sensors located on six rings throughout the whole aft shroud.

So now we can easily define the following temperatures, all measured in degrees Celsius:

- Light Shield Temperature (T_{LS}) is the average of all the eight light shield temperatures;
- Mean Light Shield Temperature (T_{LS4}) is the average of the four light shield temperatures located on the ring closest to the secondary mirror;

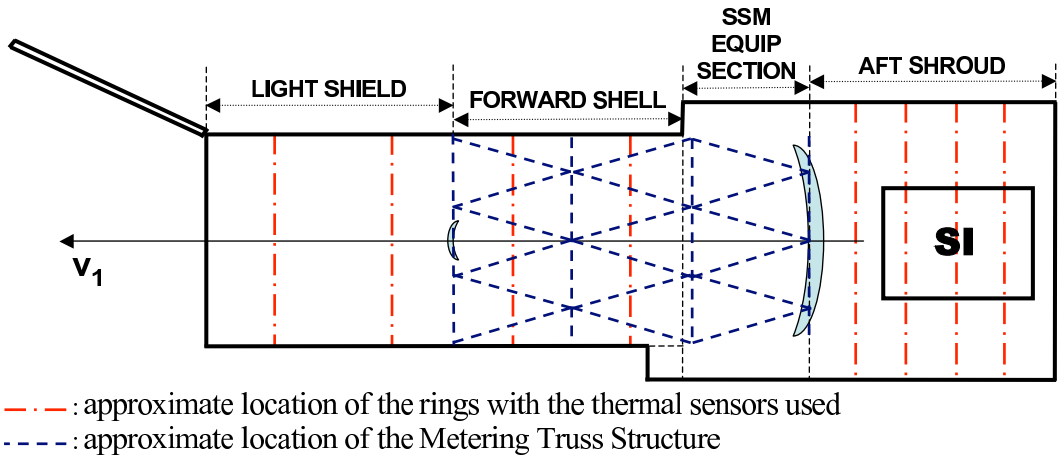

Fig. 1.— *Schematic representation of the HST main body, subdivided in four main sections with the approximate location of the temperature sensors considered in the present analysis.*

- Forward Shell Temperature (T_{FS}) is the average of the readouts of the eight thermal sensors located on two rings of the Forward Shell section;
- Truss Axial Differential Temperature (T_{MTS-ax}) is the difference between the average of the readouts of 5 MTS-sensors close to the SM and the average of the readouts of 4 MTS-sensors close to the Primary Mirror (PM);
- Truss Diametric Differential Temperature ($T_{MTS-dia}$) is the difference between the average of the readouts of 2 MTS-sensors on the $+V_2$ side of the telescope and the average of the readouts of 3 MTS-sensors on the $-V_2$ side of the telescope;
- Aft Shroud Temperature (T_{AS}) is the average of all the 14 aft shroud temperatures.

Science Data

To quantify the correlation between the focus position and the spacecraft temperature, we use two GO datasets taken with the Wide Field Channel (WFC) of the Advanced Camera for Survey (ACS) at different epochs and with different pointings.

The first dataset consists of 254 exposures (339 seconds each) in the V filter (F606W) [proposal 9750, P.I. Sahu] that from the analysis by Sahu et al. (2007) shows a strong correlation between the FWHM of the PSF and the truss axial differential temperature as well as the truss diametric differential temperature. This dataset, originally aimed at continuously observing a star field close to the Galactic Bulge for 7 days (February 22-29, 2004) for the purpose of finding transiting extra-solar planets, is well suited for studying the

medium-short term correlation between temperature and focus position. In fact, during this time frame the sun/telescope angle has always been between 64° and 72° (see Fig. 2-left), so the temperatures exhibit a sharp change at the beginning of the observation (to adapt to the new pointing) and then remain quasi constant on a daily timescale (but showing of course orbital variations on an hourly timescale) (see Fig. 3).

The second dataset consists of 126 F606W exposures (of about 700 seconds each) [proposal 10424, P.I. Richer] of the globular cluster NGC 6397 spread over a time interval of 26 days (from March 13, 2005 to April 8, 2005) with the main science driver being the determination of the cooling age of the white dwarf sequence. In this case the exposures for the program were scheduled between other observations, thus the pointing of the telescope did not remain constant (see Fig. 2-right) and this led to significant temperature excursions in the time frame as can be seen from Fig. 4. Therefore this dataset represents an ideal complement to the first to build a general focus-temperature model.

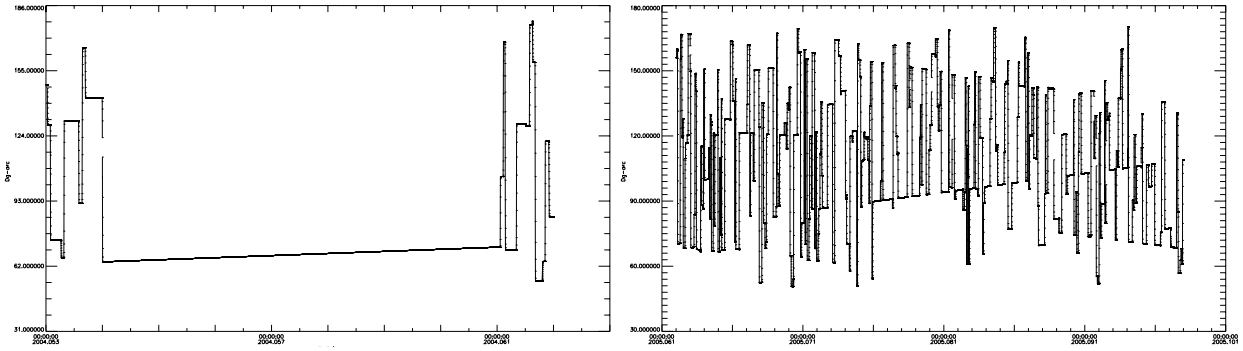

Fig. 2.— *Variation of the Sun/Telescope angle from February 22 to March 1, 2004 (left) and from March 2 to April 11, 2005 (right). [Courtesy of Tom Wheeler.]*

Measuring Focus Positions

To measure the focus positions at the time of the observations (which we set on the middle of each observation) we run the parametric (model-fitting) phase retrieval code developed by Krist & Burrows (1995) on a sample of about 20 stars for each WFC chip. The selection of the stars to be used as input for the phase retrieval is critical, in fact all the selected stars must have a high quality observed PSF as the code fits their PSFs to find the focus position. So, for each chip, we choose about 20 bright, isolated and unsaturated stars discarding, for each exposure, those affected by cosmic rays or other detector defects (such as hot pixels and bad columns). The HST focus position is then defined as the median value of the resulting focus position distribution.

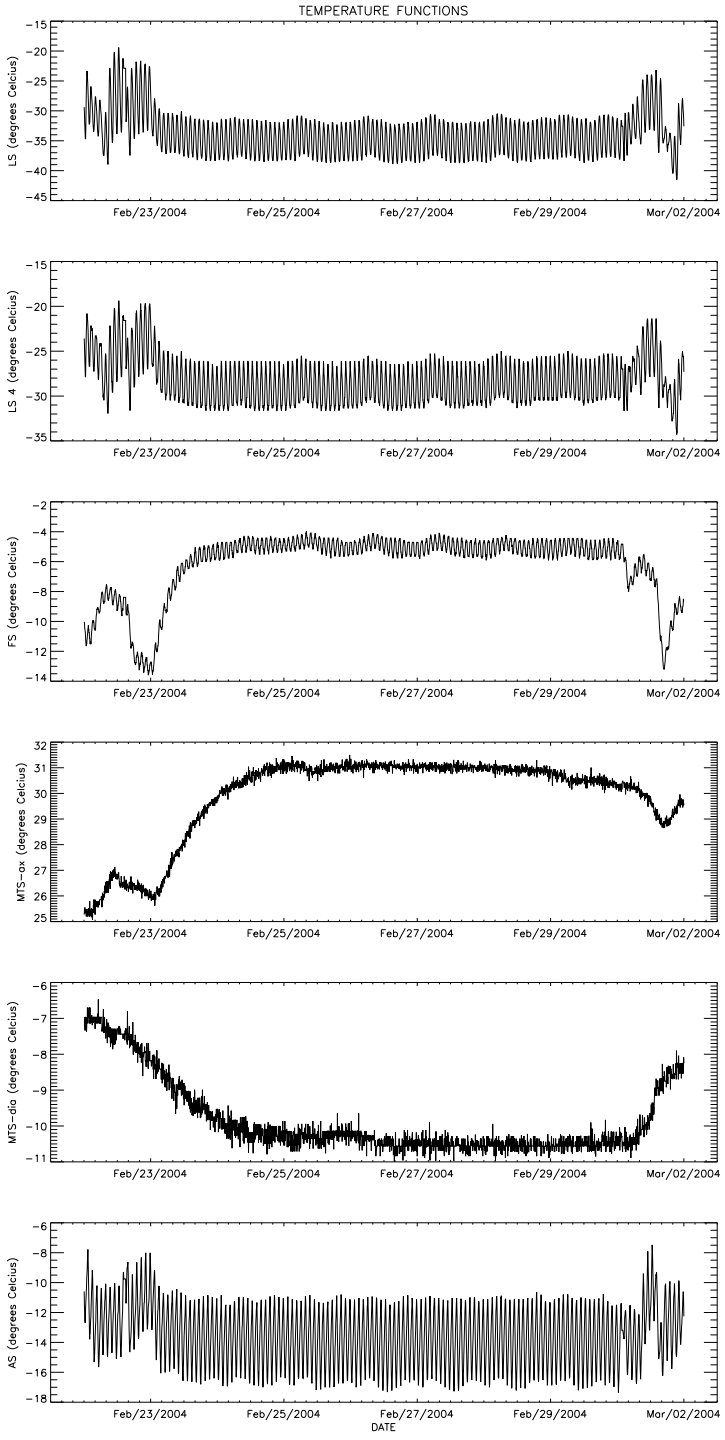

Fig. 3.— *Variation of the temperature functions during the time frame of 9750 proposal (February 22-29, 2004), from top to bottom: (i) Light Shield Temperature, (ii) Mean Light Shield Temperature, (iii) Forward Shell Temperature, (iv) Truss Axial Differential Temperature, (v) Truss Diametric Differential Temperature and (vi) Aft Shroud Temperature.*

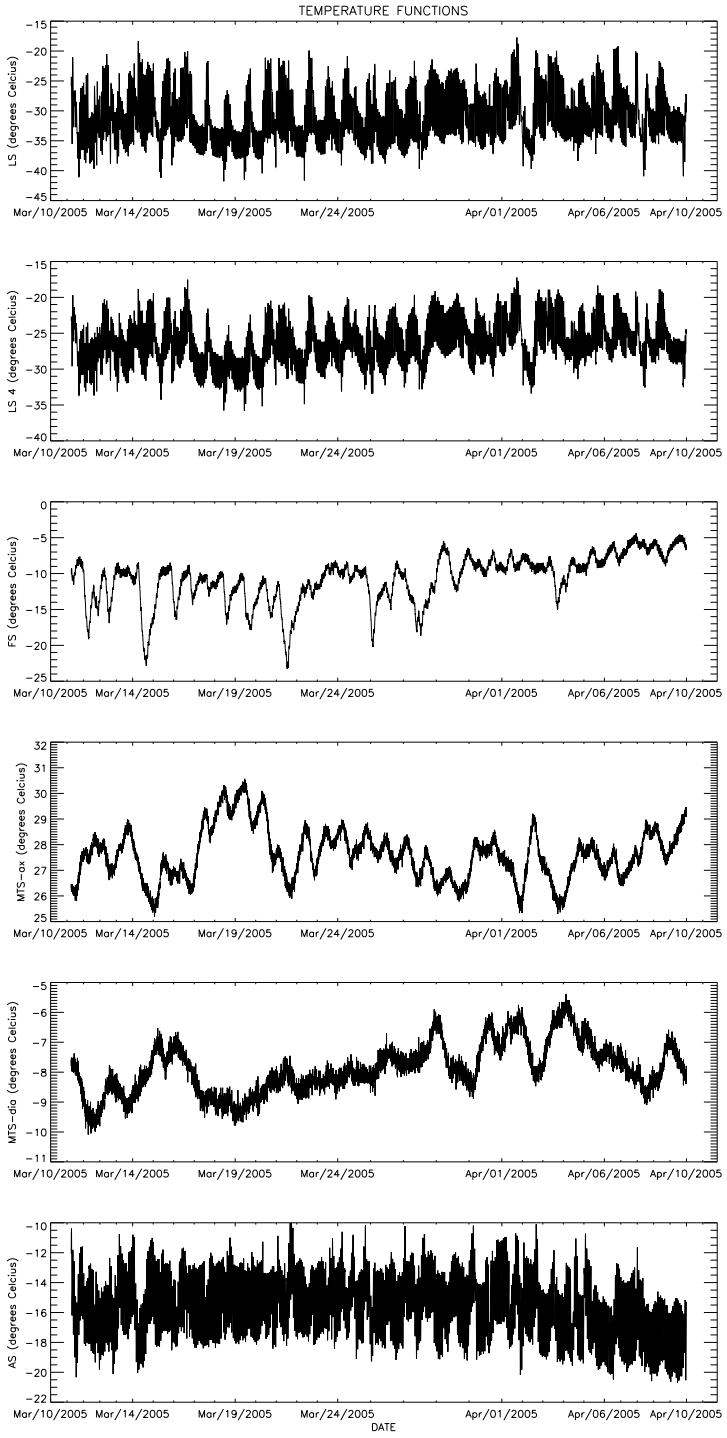

Fig. 4.— *Variation of the temperature functions during the time frame of 10424 proposal (March 13 - April 8, 2005), from top to bottom: (i) Light Shield Temperature, (ii) Mean Light Shield Temperature, (iii) Forward Shell Temperature, (iv) Truss Axial Differential Temperature, (v) Truss Diametric Differential Temperature and (vi) Aft Shroud Temperature.*

For each star, the code relies on the comparison of the observed image with a PSF-model based on an expansion in Zernike polynomials around the perfectly focused model. The best fitting coefficients of the Zernike polynomials are then mapped onto a focus displacement. Therefore from the computational point of view the problem is to find the global minimum in the multidimensional space of the fitting parameter. In the software developed by Krist & Burrows (1995) the minimization is performed iteratively using either a Levenberg-Marquart or a downhill simplex method. Unfortunately both methods are prone to achieve convergence in a local rather than global minimum depending on the initial guess parameters (see Fig. 5). To help alleviate this problem we have opted to perform the phase retrieval in each image starting from a grid of initial guess values for the focus and then selecting among all the results the one with the minimum chi-square. The code has another limitation, which is harder to overcome. In fact, it assumes that the only source of distortion in the observed PSF is due to focus related optical aberrations. In reality it is known that electronics can affect the observed PSF (see e.g., Krist 2003).

Throughout this report, the focus position is expressed in terms of microns of displacement of the secondary mirror (dSM) from its nominal (in focus) position with the convention that a negative displacement means that the secondary mirror has moved closer to the pri-

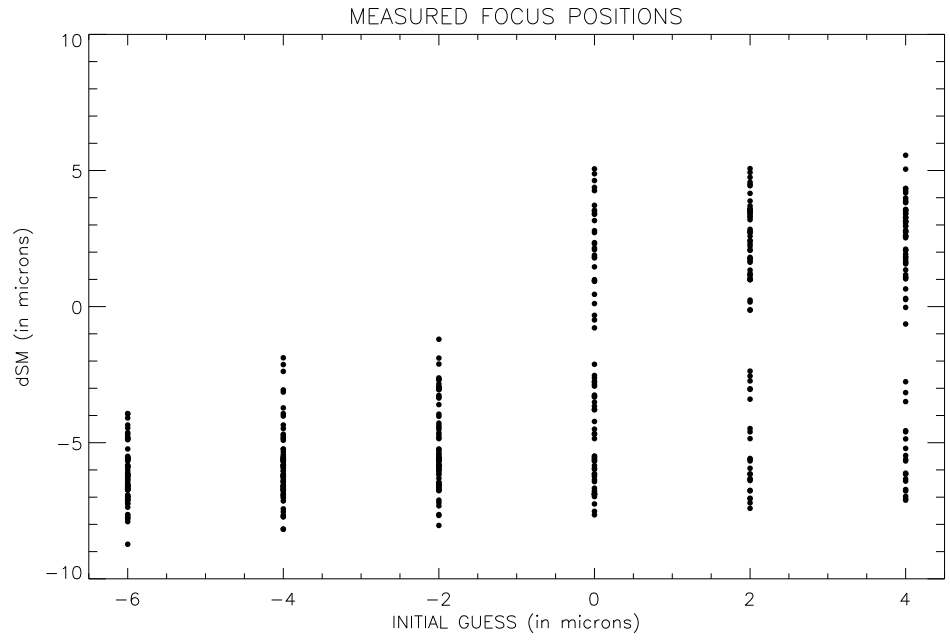

Fig. 5.— *Example of how the initial guess on the focus position affects its measurement through the phase retrieval. In the plot each dot corresponds to the focus position given by a single star on the first 3 exposures of the 9750 dataset (chip1).*

mary mirror. For historical reasons a $dSM = 0$ is currently defined as the WFPC2/PC best focus for PSFs in the 400-800 nm range. Another way to express the focus position is in terms of microns of rms wavefront error, which can be obtained by multiplying the dSM value by 0.00613 (see also Appendix B). Due to the secular shrinking of the telescope structure, the secondary mirror is constantly moving toward the primary, so in time secondary mirror moves have been commanded to compensate for this trend, in particular, during ACS lifetime the secondary mirror has been moved back by:

- 3.6 μm on December 2nd, 2002;
- 4.16 μm on December 22nd, 2004;
- 5.34 μm on July 31st, 2006.

The procedure just described allow us to determine the focus position (dSM) for both our datasets with an uncertainty of about 0.5 microns and its variation during the observation time frames is shown in Fig. 6. From the analysis we note a systematic offset between the two ACS/WFC chips:

$$\Delta(dSM) = dSM_{chip2} - dSM_{chip1} = (0.65 \pm 0.06)\mu m. \quad (1)$$

This offset is not surprising as the two chips have different focal planes by design. In the following, we analyze the focus data using both chips together after correcting the chip2 data for the offset given in eq. (1).

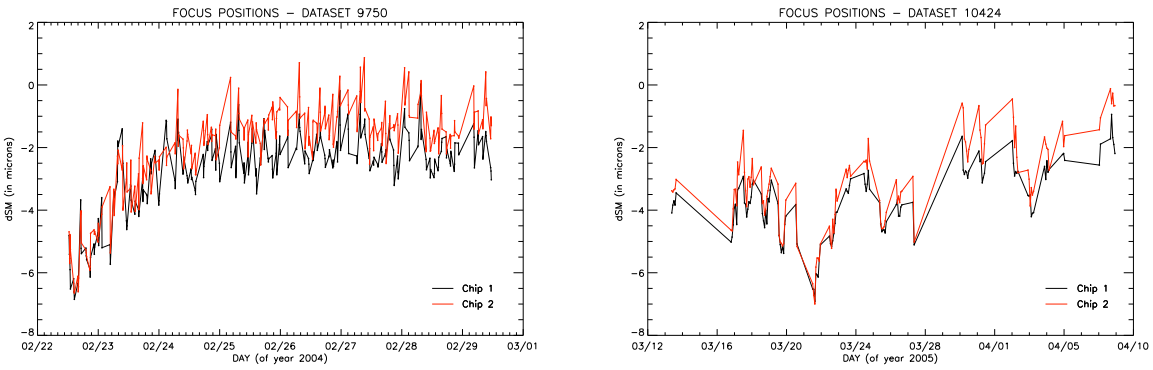

Fig. 6.— *Variation of the focus position as seen by the ACS/WFC chip1 (black line) and chip2 (red line) from February 22 to February 29, 2004 (left) and from March 13 to April 8, 2005 (right).*

Analysis

In this section we report the details of the analysis that led us to our final focus-temperature relation. We start by considering the two previously described GO datasets to model the medium-term behavior of the focus and then we describe how we use the historical monthly focus measurements to extend the validity of the model over both shorter and longer timescales.

Medium-Term Behavior

Following Hershey's work (1997), we perform a linear regression of the focus data using the 6 previously introduced temperature functions plus a 'breathing' component (T_{breath}):

$$dSM = K + \alpha_1 \cdot T_{LS4} + \alpha_2 \cdot T_{MTS-ax} + \alpha_3 \cdot T_{MTS-dia} + \alpha_4 \cdot T_{AS} + \alpha_5 \cdot T_{FS} + \alpha_6 \cdot T_{LS} + \alpha_7 \cdot T_{breath} \quad (2)$$

with K = constant and $T_{breath} = 0.7(T_{LS4} - < T_{LS4} >)$ where $< T_{LS4} >$ is the time average of the mean light shield temperature over the previous orbit, according to Bély's model (1993).

We run the linear regression first on the data from proposal 9750 and then, with the obtained coefficients, we test the formula on the data from proposal 10424, allowing re-adjustment of K. In both cases we get a very good data-model agreement, i.e. between 0.5 and 0.6 microns of error at 1 sigma for each datapoint in both chips. The same error is present also when we adopt a complementary approach by constraining the model through the 10424 data and then applying it to the 9750 data. We note that the set of coefficients in this second case is different from the previous determination; however the fit is equally good, meaning that there is degeneracy in the parameter space of the fitting coefficients. The degeneracy arises from a partial correlation among the different temperature functions, in fact, not only some of them are defined using a common subset of thermal sensors but also the heating up or cooling down of an area of the spacecraft is likely to affect the others.

In order to maximize the information present in the data for the purpose of determining the final coefficients, we perform the final linear regression using both datasets together. In this case, to take into account the focus adjustment occurred in December 2004, we introduce an offset of the form $(\gamma \cdot R)$ in eq. (2), where R is a step function:

$$R = \begin{cases} 0 & \text{for 9750 data} \\ 1 & \text{for 10424 data.} \end{cases} \quad (3)$$

In addition, as the temperature functions are correlated, it is possible that using all of them does not significantly improve the fit. For this reason, we try different combinations of temperatures, varying the number of free parameters in our model. Application of the

likelihood ratio test identifies the minimal statistically significant model as the one where the $T_{MTS-dia}$, T_{LS} and T_{breath} are set to zero, i.e.:

$$dSM \propto \beta_1 \cdot T_{LS4} + \beta_2 \cdot T_{MTS-ax} + \beta_3 \cdot T_{AS} + \beta_4 \cdot T_{FS}. \quad (4)$$

For this restricted model the total 1σ error is only 0.2% larger than the one found with the complete set of temperatures and the resulting coefficients, their errors at 1σ and their relative weights (defined as the ratio between the coefficient and its formal error at 1σ) are listed in Table 1. As the weight for the Truss Axial Differential Temperature is the largest one, we can assert that on these timescales, this temperature function is certainty the main tracker of the focus behavior, in agreement with the results of Sahu et al. (2007).

We note that the rejection of the T_{breath} term by the likelihood ratio test is most probably due to the fact that (i) 10424 data are under-sampled with respect to the 'breathing' and (ii) despite 9750 data are adequately sampled, the value of $< T_{LS4} >$ remains about constant during this time frame, so that T_{breath} can be expressed through K and T_{LS4}. The model needs to be augmented with high frequency data to reliably predict sub-orbital (< 1 hour) focus displacements. This is done in the next section.

component	coefficient	1 σ error	weight
T_{LS4}	$\beta_1 = 0.48$	0.02	24
T_{MTS-ax}	$\beta_2 = 0.81$	0.03	27
T_{AS}	$\beta_3 = -0.28$	0.02	14
T_{FS}	$\beta_4 = 0.18$	0.015	12

Table 1: *Coefficients for eq. (4) found through a linear regression with data of both 9750 and 10424 proposals, with correspondent errors at 1σ and weights.*

Short-Term Behavior

As described by Bély (1993) and Lallo (2005), the HST focus shows hourly variations (breathing) due to the orbital position of the telescope. To include this behavior in our model, we use the historical (from March 2003 to October 2007) focus data obtained to monitor the displacement of the secondary mirror because they have the required high-frequency. In fact, to collect these data, almost every month a star cluster (47 Tuc or M35) is observed with parallel exposures in ACS/HRC and WFPC2/PC (so that a bright star is always near the center of the two apertures) using the F550M filter for HRC and the F547M filter for PC.

Each month, the observation lasts one single orbit with alternating ACS/HRC exposures of 3.0 s and WFPC2/PC exposures of 1.0 s and at the end of the nominal orbit, one single ACS/WFC 8.0 s exposure is sometime taken with the F502N filter. As ACS/WFC data are more sporadic and are affected by a larger observational error, we use them only to check our results and not to build the model itself.

Our temperature model of the focus variations is in principle applicable to instruments different from ACS/WFC because we are considering thermal sensors located in the common structure of the spacecraft. Nevertheless, it is important to note that:

(i) the monthly focus observations are taken with different filters than the one used to obtain the model, but the phase retrieval software used to determine the focus accounts for the wavelength dependence and produces a result that is given in waves at a specific wavelength that we then convert to a physical displacement of the SM;

(ii) the estimated error of the focus measurements (always conducted through the parametric phase retrieval code) for these data is larger (being about 1 μm) than the one obtained previously with the GO datasets as only one star is observed;

(iii) different science instruments may need different values of the constant term (K). This constant term can also vary in time due to the commanded focus adjustments and other long-term effects (e.g., outgassing).

From point (iii) it follows that, in order to find the coefficients for the breathing component through the use of historical data, it is better to analyze each camera and each month separately. So for each subset of data we subtract the value of the focus predicted by our four-temperature model [eq. (4)] from the observed focus value and we fit this quantity as a linear function of T_{breath}:

$$dSM_{obs} - dSM_{pred} \propto \alpha \cdot T_{breath}. \tag{5}$$

Then we average all the resulting values of the coefficient α and we get $\alpha = 0.55 \pm 0.25$. Adding this term back to our four-temperature model, allows us to calibrate the constant with our original GO datasets and the results, plotted in Fig. 7 and Fig. 8, show that the observed focus position is recovered within its observational error (0.5-0.6 μm) by the following formula:

$$dSM = K' + 0.48 \cdot T_{LS4} + 0.81 \cdot T_{MTS-ax} - 0.28 \cdot T_{AS} + 0.18 \cdot T_{FS} + 0.55 \cdot T_{breath} \tag{6}$$

with

$$K' = \begin{cases} -14.96 & \text{for 9750 data (ACS/WFC chip1)} \\ -15.14 & \text{for 10424 data (ACS/WFC chip1).} \end{cases} \tag{7}$$

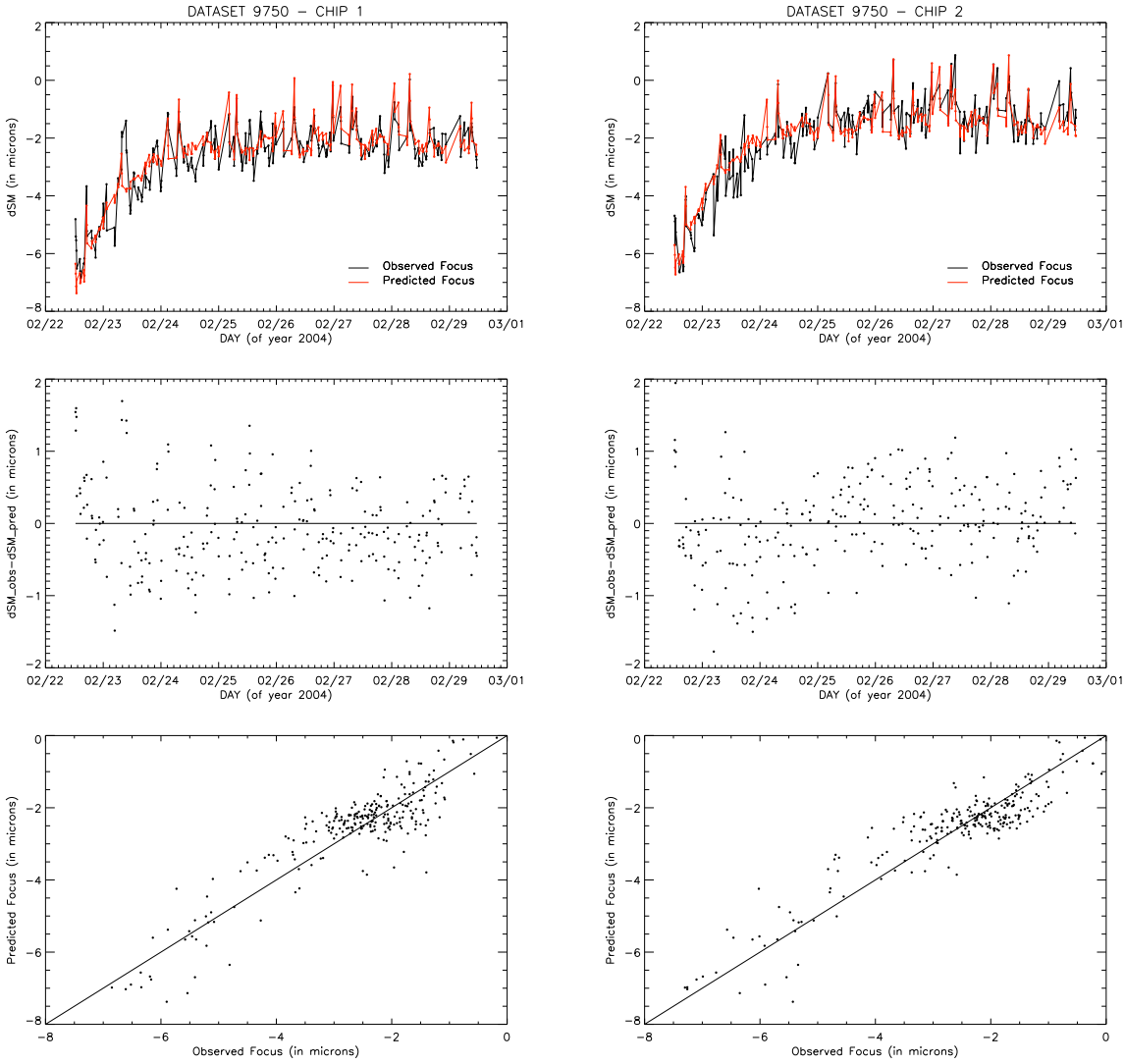

Fig. 7.— *Comparison between the focus positions observed from February 22 to February 29, 2004 (chip1 on the left, chip2 on the right) and the focus positions predicted through the model described by eq. (6).*

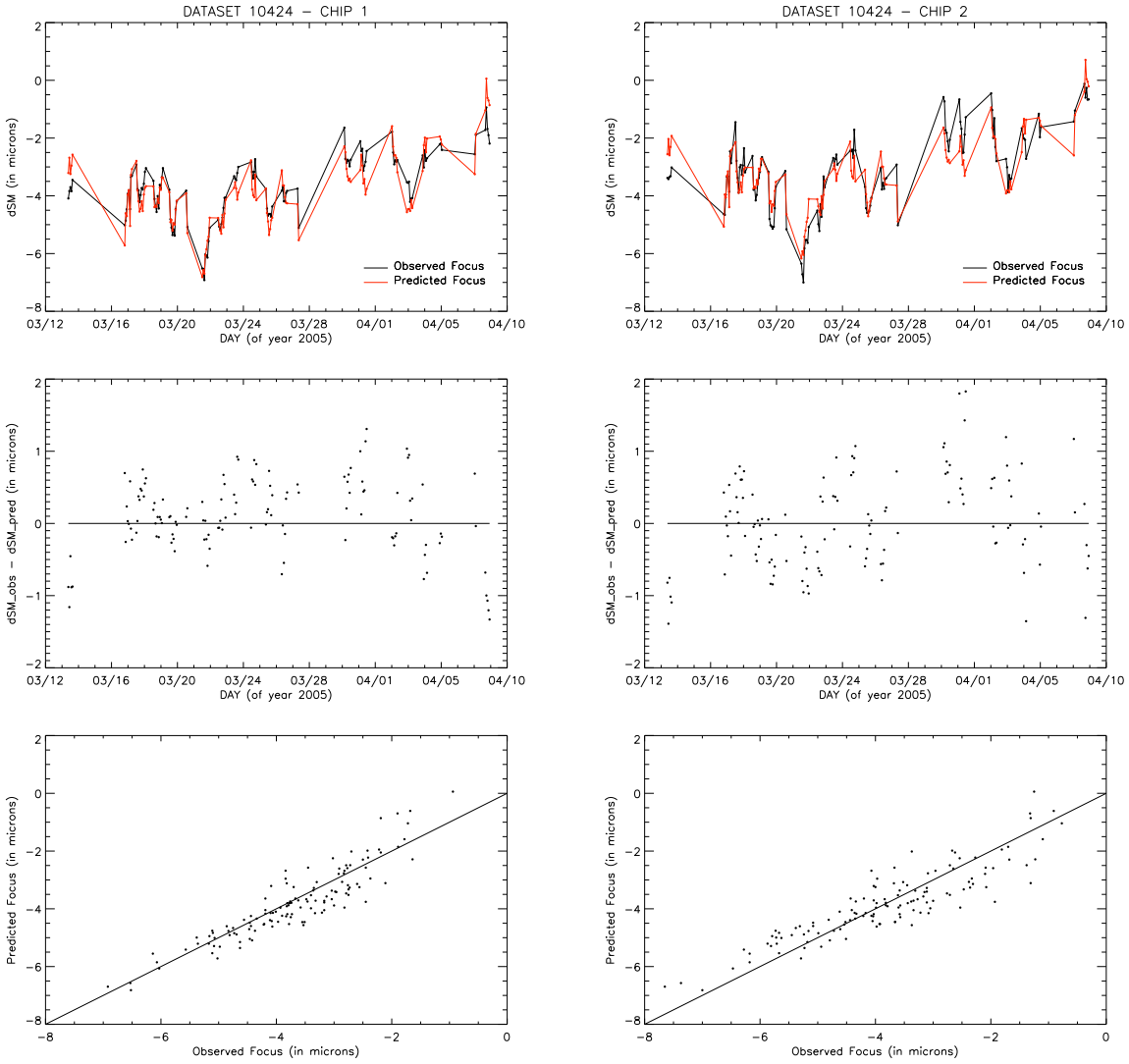

Fig. 8.— *Comparison between the focus positions observed from March 13 to April 8, 2005 (chip1 on the left, chip2 on the right) and the focus positions predicted through the model described by eq. (6).*

Long-Term Behavior

We need to emphasize that eq. (6) is valid for timescales of about 2 months, where focus variations are mainly due to temperature changes, but a more complete characterization of the focus position requires taking into account also long-term effects, like the overall shrinking of the telescope structure due to gas desorption. This effect is purely mechanical and thus it is possible to study its behavior once the fluctuations due to temperature have been subtracted. In order to include this effect and validate the model over longer timescales, we again make use of the historical focus data. This time, as the shrinking is a long term effect (about 9 μm in 5 years), we consider only the mean focus value over each orbit and we use all the monthly data together after correcting for the commanded focus adjustments, again choosing the focus position of 2003 (same as for the 9750 dataset) as 'zeropoint' (see Fig. 9).

For each camera separately we subtract the focus predicted by our model [eq. (6)] from the observed focus position, fit the resulting difference with a linear function of time and then average the coefficients thus obtained. This approximation yields the following description

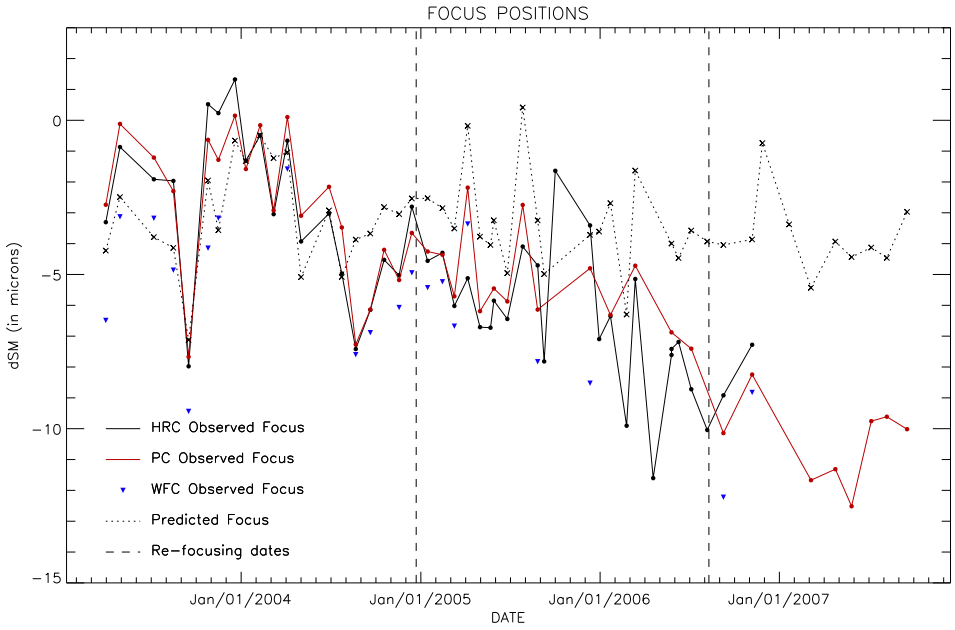

Fig. 9.— *Focus positions from March 2003 to October 2007 as measured with ACS/HRC (black line), with WFPC2/PC (red line) and with ACS/WFC (blue dots) compared with the predictions of the model developed for ACS/WFC (dotted line) given by eq. (6). The model was calculated at the date and time of each measurement, but for each month only the average focus position over one orbit is plotted.*

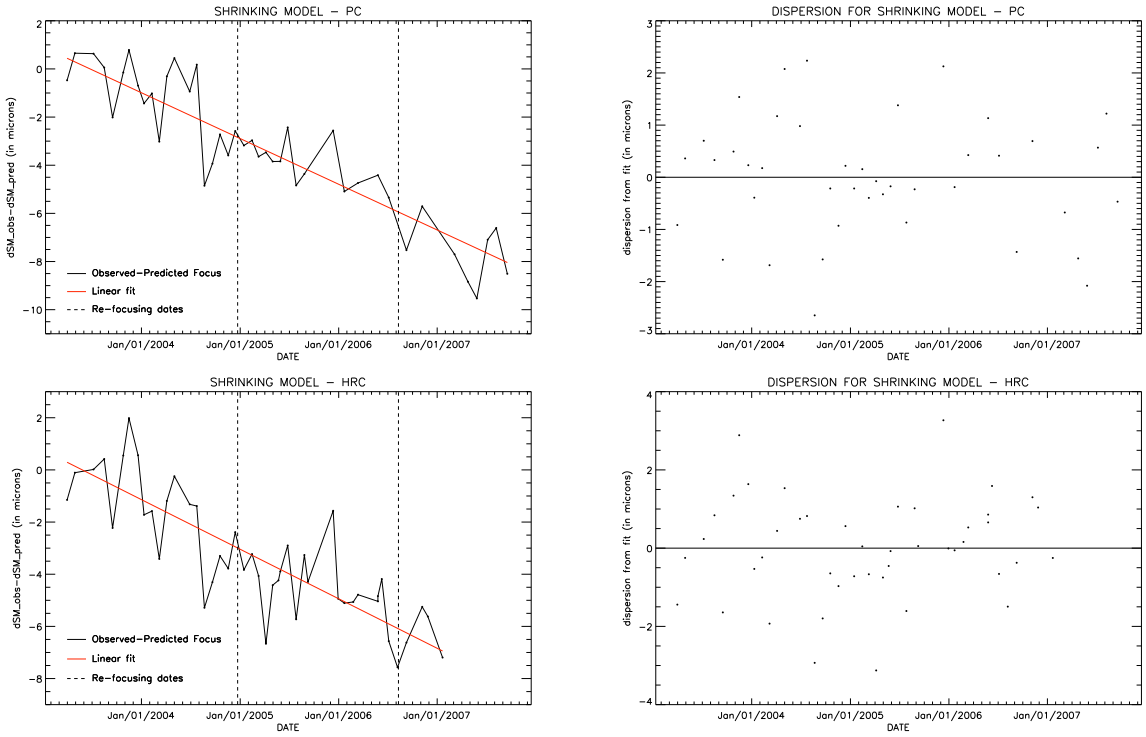

Fig. 10.— *Shrinking trend (black line) obtained by subtracting the focus positions predicted through eq. (6) from the observed focus positions (collected from March 2003 to January 2007/October 2007) and its linear fit (red line) for WFPC2/PC data (top) and ACS/HRC data (bottom) with the correspondent dispersion plotted on the right.*

of the shrinking (valid only after March 2003):

$$dSM_{obs} - dSM_{pred} \propto -0.0052(\pm 0.0004) \cdot MJD \tag{8}$$

where MJD is the time of the observation expressed as Modified Julian Date (e.g. May 26, 2006 at 8:49:16am UT = 53881.36755). As shown in Fig. 10, the shrinking trend shows wide variations, but its linear characterization presents an error at 1σ of 1.1 μm, which is comparable with the observational error (1 μm).

Final Model

Putting together eq. (6) and eq. (8) we obtain the complete model of the focus variations:

$$dSM = C - 0.0052 \cdot MJD + 0.48 \cdot T_{LS4} + 0.81 \cdot T_{MTS-ax} - 0.28 \cdot T_{AS} + 0.18 \cdot T_{FS} + 0.55 \cdot T_{breath} \tag{9}$$

where the constant C is:

$$C = \begin{cases} 261.10 & \text{for WFPC2/PC data} \\ 261.00 & \text{for ACS/HRC data} \\ 259.70 & \text{for ACS/WFC - chip 1 data} \\ 260.35 & \text{for ACS/WFC - chip 2 data.} \end{cases} \tag{10}$$

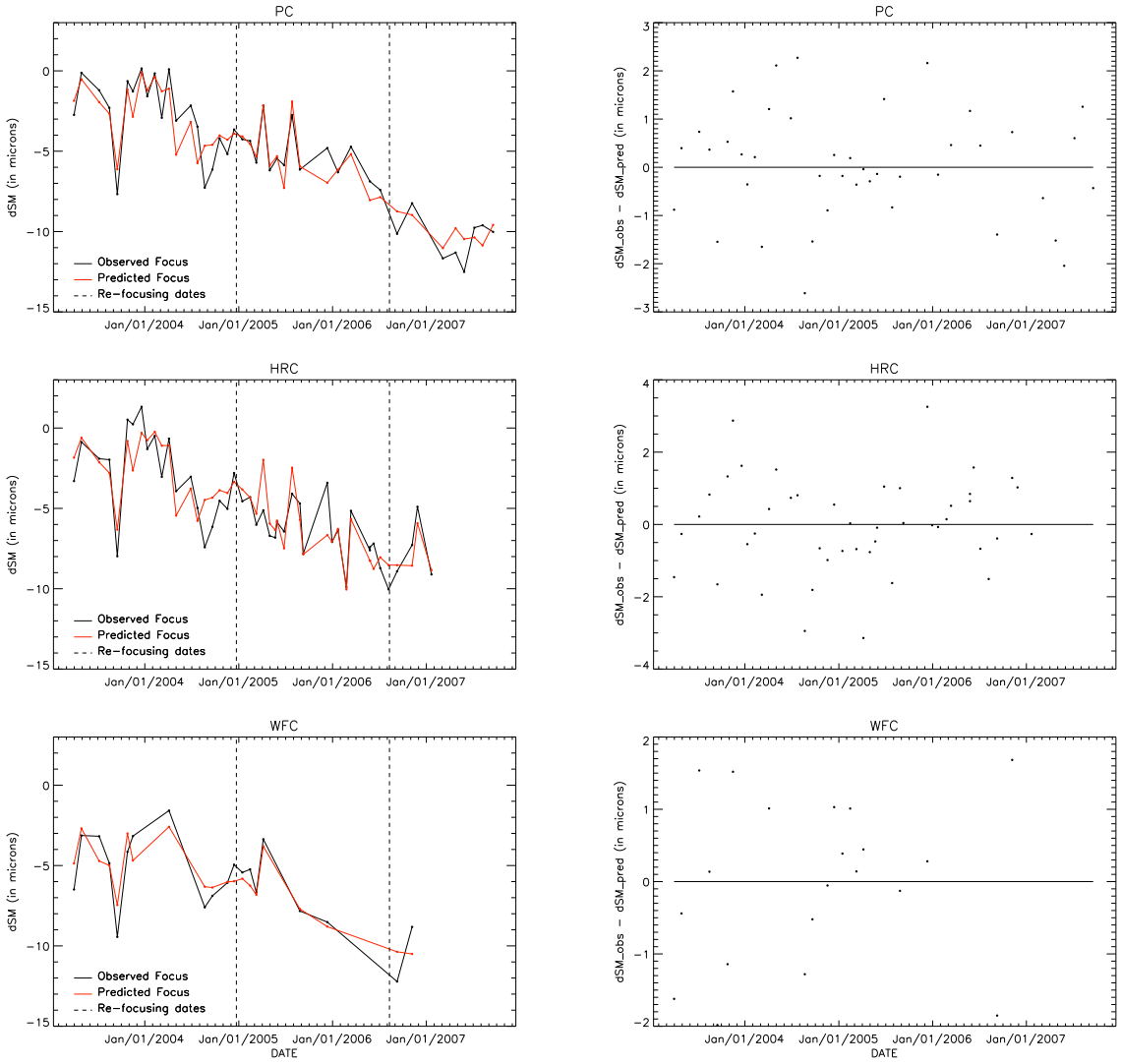

Fig. 11.— *Comparison between our temperature model of focus variations described by eq. (9) and eq. (10) with the observed data (collected from March 2003 to January 2007/October 2007) for WFPC2/PC (top), ACS/HRC (middle) and ACS/WFC (bottom) with the correspondent dispersion plotted on the right.*

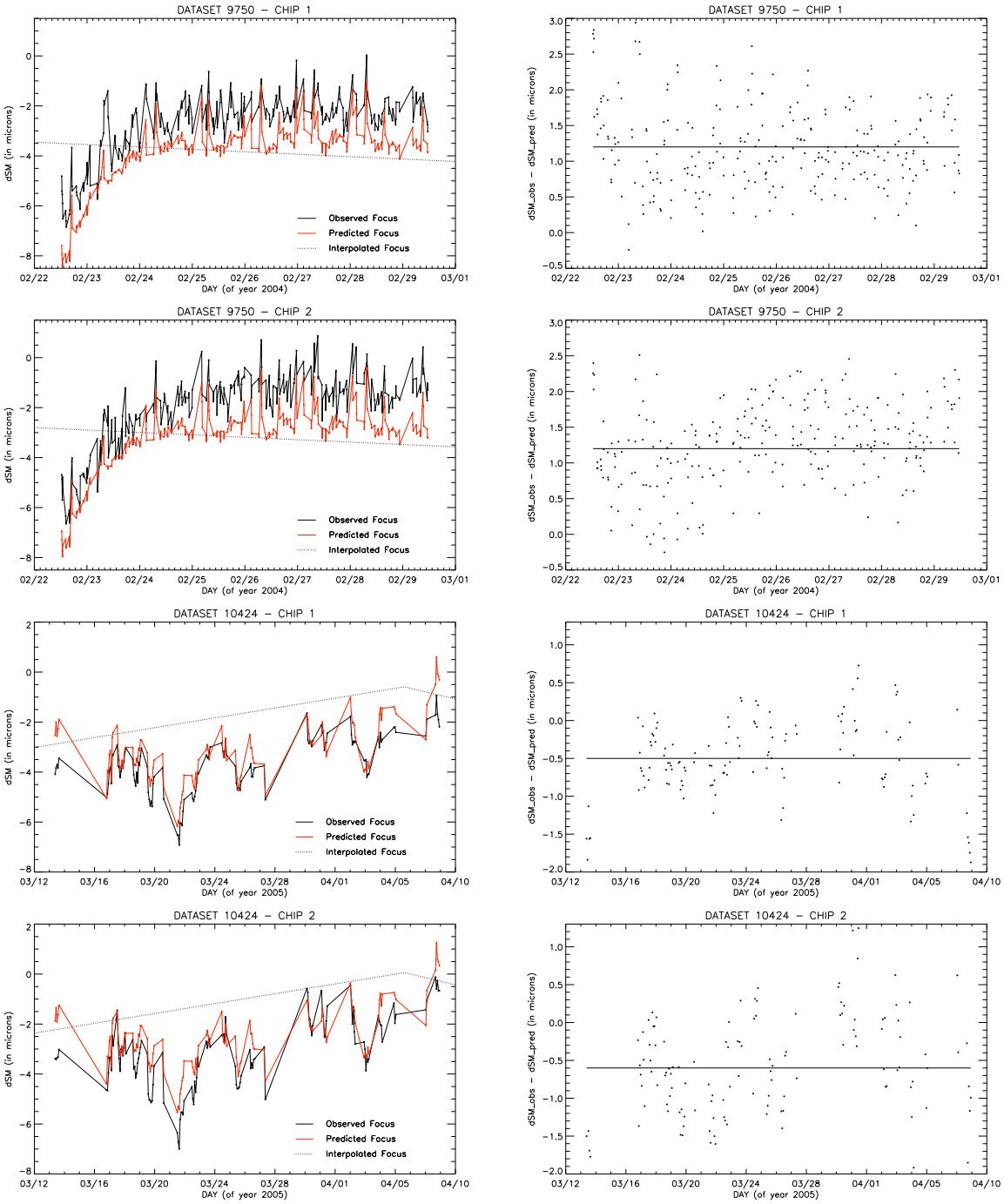

Fig. 12.— *Comparison between our temperature model of focus variations described by eq. (9) and eq. (10) [red line] with the observed data [continuous black line] and with the focus found with a linear interpolation of the historical data [dotted black line]. The corresponding dispersion is plotted on the right. From top to bottom: data from 9750 proposal (February 22-29, 2004) chip1 and chip2, data from 10424 proposal (March 13 - April 8, 2005) chip1 and chip2.*

This model includes effects that may happen on all the previously discussed timescales and therefore should be of general validity. To test this statement on long timescales, we apply the model described by eq. (9) with the offsets listed in eq. (10) to the time of the historical data and for each instrument the resulting predicted focus (plotted in Fig. 11) is in very good agreement with the observed focus positions, in fact the error at 1σ is 1.1 μm for WFPC2/PC data, 1.2 μm for ACS/HRC and 1.3 μm for ACS/WFC.

Then we apply the model [eq. (9) and (10)] again to the data from the 9750 and 10424 proposals and we notice (as highlighted in Fig. 12) a systematic offset in the focus positions of about 1.2 μm for the 9750 data and of about -0.55 μm for the 10424 data. This is most probably due to the fact that we described the shrinking model through the historical data with a linear approximation that is certainly good enough to describe the overall evolution, but locally there can be discrepancies which represent the dominant error component.

This means that without proper modeling of the shrinking the usefulness of our model remains limited to periods of about two months (in fact we recall that the average shrinking is 0.3 μm over two months). However it is important to note that our temperature model has the unique capability of capturing high frequency variations of the focus positions, which cannot be modeled using the historical focus data alone (taken monthly). For example, in both the high frequency datasets that we consider there are variations of the focus greater than 6 μm in less than one week. The linear interpolation of historical data gives instead variations below 1 μm on a weekly timescale (dotted black line in Fig. 12).

In addition our temperature model is also able to reproduce short-term variations of the focus position. In fact it is clearly evident that our temperature model performs at least as well as the only previously known model (Bély 1993) by looking at Fig. 13, which shows a comparison between the focus predicted by the two formulae (after proper calibration of the constant term for both of them) and at Table 2, which reports the corresponding dispersion values for a sample of historical data.

Thus we can conclude that our model is able to reproduce focus variations with an error of about 1.5 μm if used with the constant term provided by eq. (10), but it becomes even more accurate if the data allow the calibration of the offset.

		rms obtained with	
		our model	Bély's model
PC	20 September 2004	0.25	0.33
	29 May 2005	0.31	0.22
HRC	22 May 2005	0.32	0.38
	30 December 2005	0.34	0.23

Table 2: *Dispersion from observed focus positions obtained by applying both our temperature model and Bély's breathing formula (after proper calibration of the constant term for both models) for a sample of historical data.*

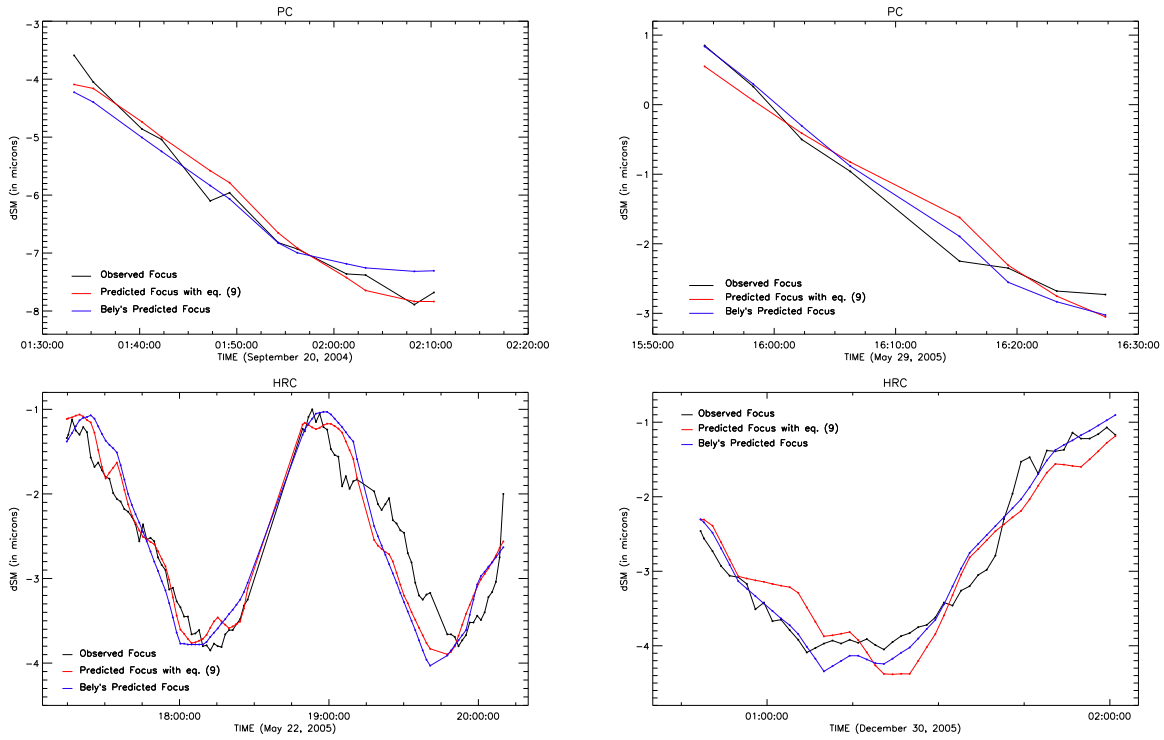

Fig. 13.— *Comparison between the focus positions predicted by our temperature model (red line) and those predicted by Bély's model (blue line); the constant term was properly calibrated for both models. The observed focus positions are also plotted (black line). TOP-LEFT: WFPC2/PC data obtained on September 20, 2004. TOP-RIGHT: WFPC2/PC data obtained on May 29, 2005. BOTTOM-LEFT: ACS/HRC data obtained on May 22, 2005. BOTTOM-RIGHT: ACS/HRC data obtained on December 30, 2005.*

Conclusions

In this report we investigate the relation between focus and temperature variations in HST. For this we take advantage of (i) the data from two independent GO programs that imaged hundreds of times the same stellar field, contiguously for one week in one case and with repeated visits spread over one month in the other case; (ii) the archived historical HST focus measurements (a single star imaged several times over a single orbit once each month) which extends over multiple years. The GO data allow us to determine the focus position via parametric phase retrieval performed on more than 10 stars per exposure, which gives a combined 1σ focus constraint better than $0.5\mu m$. A linear regression with four temperatures reproduces the focus variations at about the same accuracy of the focus measurement and the parameters of the model estimated on one dataset fit well the other. Despite the fact that historical focus data have a larger observational error ($\sim 1\mu$m), when analyzed month by month, they allow us to calibrate the breathing term, validating the model even on orbital timescales.

On timescales longer than a couple of months, temperature changes alone cannot explain the focus variations as other effects can be in play, such as outgassing of the spacecraft which leads to a progressive shrinking of the metering truss. If we introduce an approximate linear model of the shrinking combined with our temperature model, the historical focus variations are then recovered to about 1 μm accuracy. However if the shrinking model, fixed on the historical data, is applied to the two GO datasets (with higher frequency data), then we notice a systematic offset in the focus at $1\mu m$ level. Most probably this is because the shrinking is a point random process, thus a linear model is realistic only over timescales much longer than that of the point process.

Nevertheless our final model overperforms a linear interpolation of historical data, given its capability of capturing short term, high frequency variations of the focus position and reproduces orbital focus oscillations as well as the only previously known short-term model (Bély 1993).

To further improve the focus modeling, one should consider that in addition to the effects discussed in this ISR, there may be other processes that contribute to influence the position of the focus. For example hysteresis and/or persistence effects (different from the one already included in the breathing term) may contribute or the detector electronic may be responsible for additional variations. The location of the temperature sensors we use may also introduce biases as we limit ourselves to spacecraft sensors. A future improvement upon our work might consider including temperatures measured closer to the HST instruments. One other possible way to improve the modeling is that of acquiring high frequency quality dataset for the purpose of measuring the focus. If future science programs will happen to

carry out observations with the desired properties, the present model could be validated over a longer timescale and in case improved upon.

Acknowledgments

We thank Tom Wheeler and Joshua Abel for sharing their engineering expertise on the HST structure and thermal system. We are also very grateful to Michele Trenti for the countless useful discussions and to Roeland Van der Marel and Chris Long for their technical advices and help in the preparation of the web interface that we are developing.

References

Anderson, J. & King, I.R. 2003, PASP, 115, 113

Bély, P.Y., Hasan, H. & Miebach, M. 1993, "Orbital Focus Variations in the Hubble Space Telescope", SESD-93-16,6/93 (Baltimore:STScI)

Ciardullo, R., Bond, H.E., Sipior, M.S., Fullton, L.K., Zhang, C.-Y. & Schaefer, K.G. 1999, AJ , 118, 488

Hamilton, T.S., Casertano, S. & Turnshek, D.A. 2008, ApJ (in press), arXiv:0802.1786

Hasan, H. 1993, "Pre-COSTAR Status of OTA Focus", ISR OTA 1993-14 (Baltimore:STScI)

Hasan, H., Burrows, C.J. & Schroeder, D. 1993, PASP, 105, 1184

Hershey, J.L. 1997, "Modeling HST Focal-Length Variations", SESD-97-01,6/98 (Baltimore:STScI)

Krist, J. 2003, "ACS WFC & HRC Field-dependent PSF Variations due to Optical and Charge Diffusion Effects", ISR ACS 2003-06 (Baltimore:STScI)

Krist, J. & Burrows, C.J. 1995, "Phase-Retrieval Analysis of pre- and post-repair Hubble Space Telescope Images", Appl. Opt. **34**, 4951-4964

Krist, J. & Hook, R. 2004, "The Tiny Tim User's Guide", Version 6.3 (Baltimore: STScI)

Lallo, M., Makidon, R.B., Casertano, S., Gilliland, R. & Stys, J. 2005, "HST Temporal Optical Behavior and Current Focus Status", ISR TEL 2005-03 (Baltimore:STScI)

Martel, A.R., et al. 2003, AJ, 125, 2964

McNeil, S.R., & Moody, J.W. 2005, ApJ, 627, 701

Park, Y., Casertano, S., & Ferguson, H.C. 2004, ApJ, 600, L159

Remage Evans, N., Schaefer, G.H ., Bond, H. E., Bono, G., Karovska, M., Nelan, E., Sasselov, D. & Mason, B. 2007, American Astronomical Society Meeting Abstracts, 211, 03.23

Rhodes, J., Refregier, A. & Groth, E.J. 2000, ApJ, 536, 79

Sahu, K.C. et al. 2006, Nature, 443, 534

Sahu, K.C., Lallo, M. & Makidon, R.B. 2007, "ACS PSF Variations with Temperatures", ISR ACS 2007-12 (Baltimore:STScI)

Schneider, G. et al. 2006, ApJ, 650, 414

Suchkov, A. 1998, "Possible Evidence for NICMOS Focus 'Precessional Breathing' ", ISR NIC 1998-07 (Baltimore:STScI)

Yoshikawa, Y., Castro, D. & Piquero, J. 1999, "HST Thermal Control System Description and Operating Manual", LMSC/F420173B (Greenbelt:GSFC)

Appendix

A. Summary Guide for Application of the Model

Here we briefly summarize the necessary steps in order to derive the focus position for a given observation made with WFPC2/PC or ACS/WFC or ACS/HRC and executed after March 09, 2003. Note that the temperature functions used in this ISR were not routinely calculated before that date.

1. *Request temperature data* for the time interval of the observation by writing to `help@stsci.edu`.

2. *Choose the constant* to use in eq. (9). Here two different possibilities are available:

   a) use the values of the constant provided in eq. (10), keeping in mind that these values are referred to the focus position of 2003, so it can be required to correct for commanded focus adjustments;

   b) calibrate the constant term using the historical data closest to the time of the observation.

3. *Evaluate the focus position* (dSM) in terms of microns of displacement of the SM by using eq. (9).

4. *Model the observed PSF.* If the Tiny Tim software (Krist & Hook 2004) is used for this step, the focus position needs to be edited in the parameter file created by 'tiny1' at the entry 'Z4' (by the end of the file itself). For historical reasons the value of 'Z4' (4^{th} Zernike parameter) is expressed in waves of defocus at 547 nm instead of microns of displacement of the SM (see also Krist & Hook 2004). Each micron of SM displacement corresponds to 0.0112 waves of RMS focus difference at $\lambda = 547$ nm. To accurately model the defocused PSF, 0.0112 waves of defocus needs to be added or subtracted to the default Z4 term in the 'tiny1' parameter file for each micron of SM despace [e.g., $Z4_{new} = (dSM * 0.0112) + Z4$].

Note that STScI is planning to create a web tool at the following URL:

`http://www.stsci.edu/hst/observatory/focus`

that will automate the steps 1, 2a and 3 for a given date or range of dates.

B. Conversion from Secondary Mirror Despace to Waves of Defocus

From Hasan, Burrows & Schroeder (1993), we know that a 1 micron change in the SM despace (dSM) produces a corresponding displacement of the HST focal plane (ΔHST_{focus}) of ~ 110 microns via the relationship,

$$\Delta HST_{focus} = (m^2 + 1) \cdot dSM = 109.88 \cdot dSM, \tag{11}$$

where $m = f/f_1 = 24.0/2.3 = 10.435$. Here, f and f_1 are the $f\ numbers$ of the HST Optical Telescope Assembly (OTA) and the Primary Mirror respectively. The displacement of the HST focal plane can be expressed in waves of defocus via the relationship,

$$\Delta HST_{focus} = 8 \cdot (a4 \cdot Z4) \cdot f^2 \tag{12}$$

where $a4$ is the coefficient associated with the Zernike polynomial $Z4$ (focus), and f is the $f\ number$ of the HST OTA. Here, ΔHST_{focus} and $Z4$ are expressed in microns. For HST, with a SM that obscures 33% of the HST aperture, the coefficient $a4 = 3.8874443$ (HST OTA Handbook). Solving for Z4, we find 1 micron of SM motion produces 0.00613 microns of RMS wavefront error. This is equivalent to 0.0112 waves of RMS error at $\lambda = 547$ nm.

C. Location of the Thermal Sensors

In this appendix we report (i) the definitions of the spacecraft temperature functions used and (ii) the locations of the thermal sensors themselves. These main temperature functions were selected by Hershey (1997) because they show a time dependence related to the orbital phase or to the telescope attitude. In the following description, each thermal sensor is identified by an ID label starting with a capital letter and followed by a 3-digit number. Most of the information reported in this appendix can also be found in Yoshikawa, Castro & Piquero (1999), but here it has been complemented with additional information from private communications with HST engineers.

For the Light Shield section of the spacecraft (that goes from station 455.3 to station 608.5) we consider eight thermal sensors: four at station 493.8 (T307, T308, T309 and T310) and four at station 570 (T303, T304, T305 and T306). These sensors are spaced unevenly

around the circumference of the Light Shield structure as shown in Fig. 14. Using the readout values of these sensors, the Light Shield Temperature (T_{LS}) and the Mean Light Shield Temperature (T_{LS4}) are defined as follows:

$$\begin{aligned} T_{LS} &= (\mathrm{T303} + \mathrm{T304} + \mathrm{T305} + \mathrm{T306} + \mathrm{T307} + \mathrm{T308} + \mathrm{T309} + \mathrm{T310})/8; \\ T_{LS4} &= (\mathrm{T307} + \mathrm{T308} + \mathrm{T309} + \mathrm{T310})/4. \end{aligned}$$

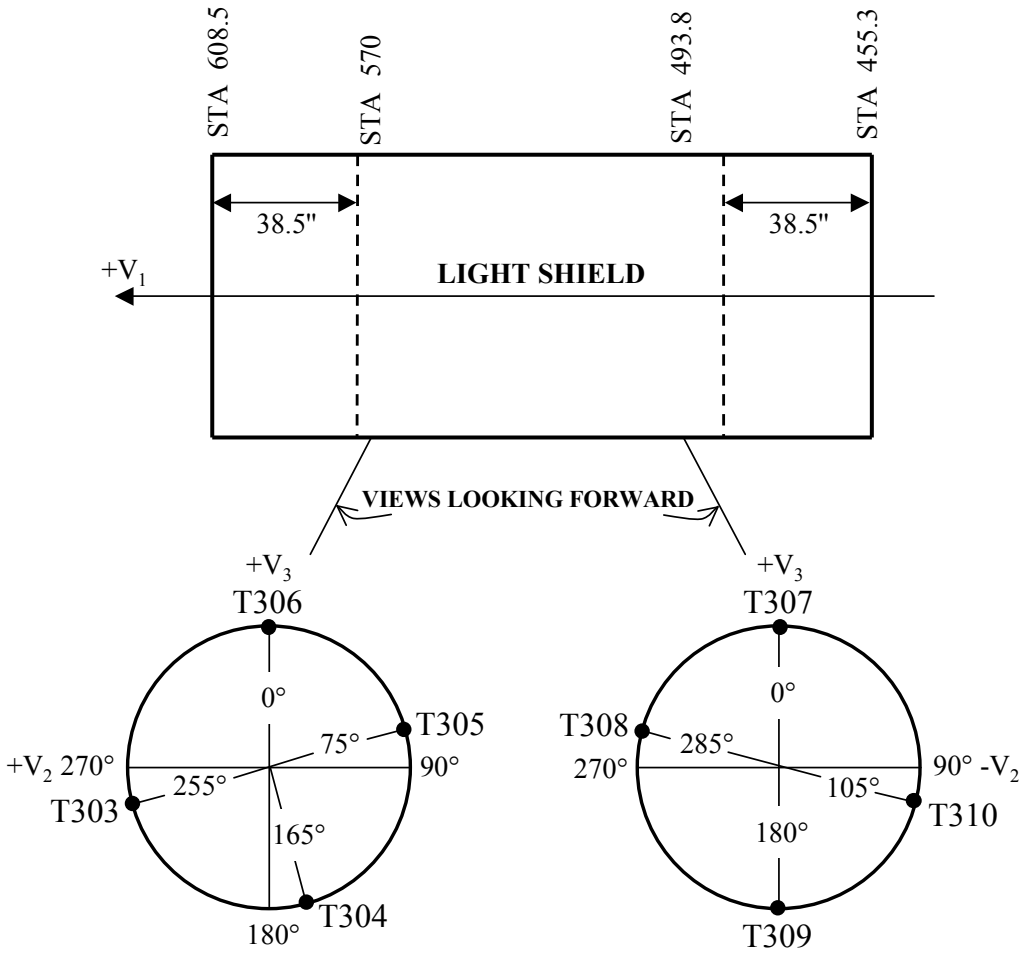

Fig. 14.— *Location of the Light Shield thermal sensors: T303, T304, T305, T306, T307, T308, T309 and T310. Angles are measured from the $+V_3$ axis toward the $-V_2$ axis. Figure 2-3 from Yoshikawa, Castro & Piquero (1999).*

For the Forward Shell section of the spacecraft (that goes from station 299 to station 455.3) we consider eight thermal sensors: four at station 342.5 (T317, T318, T319 and T320) and four at station 416.2 (T313, T314, T315 and T316). These sensors are spaced evenly at 90° intervals around the circumference of the Forward Shell structure as shown in Fig. 15. Using the readout values of these sensors, the Forward Shell Temperature (T_{FS}) is defined as follows:

$$T_{FS} \;=\; (\mathrm{T313} + \mathrm{T314} + \mathrm{T315} + \mathrm{T316} + \mathrm{T317} + \mathrm{T318} + \mathrm{T319} + \mathrm{T320})/8.$$

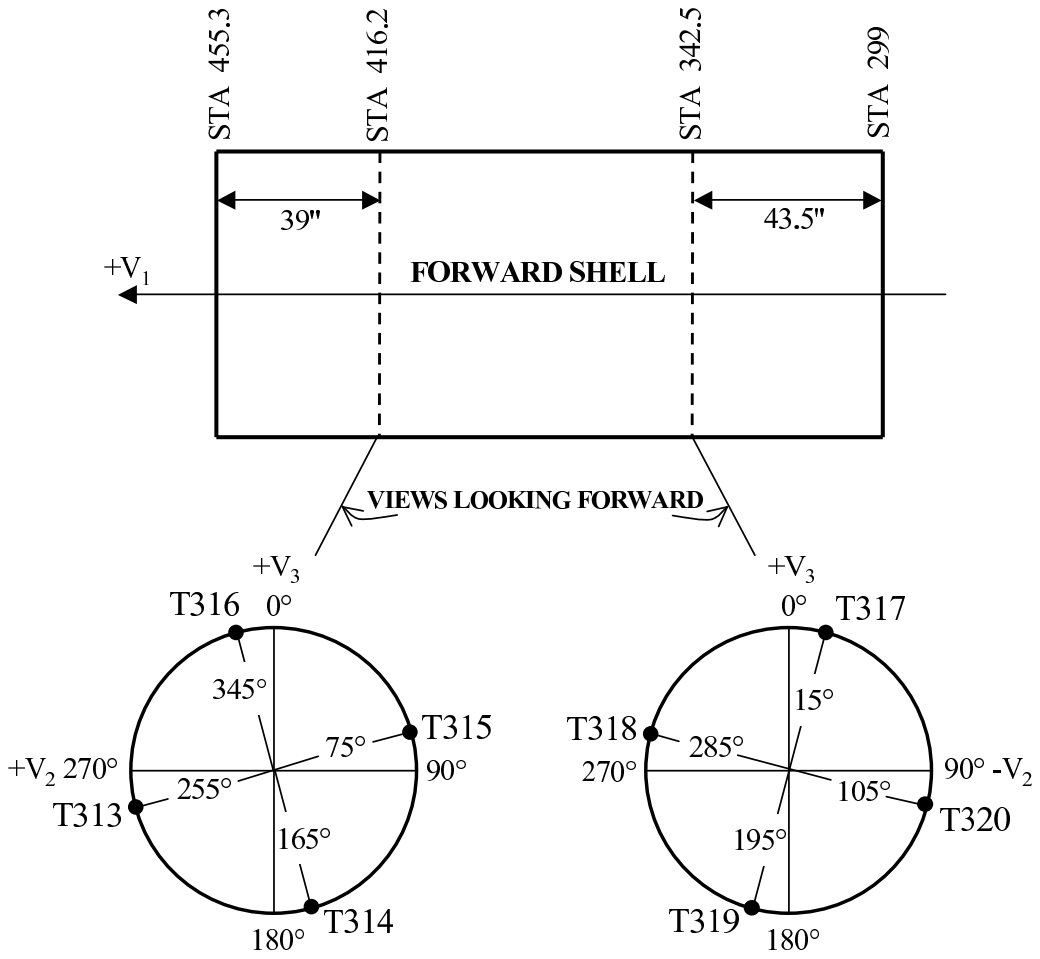

Fig. 15.— *Location of the Forward Shell thermal sensors: T313, T314, T315, T316, T317, T318, T319 and T320. Angles are measured from the $+V_3$ axis toward the $-V_2$ axis. Figure 2-4 from Yoshikawa, Castro & Piquero (1999).*

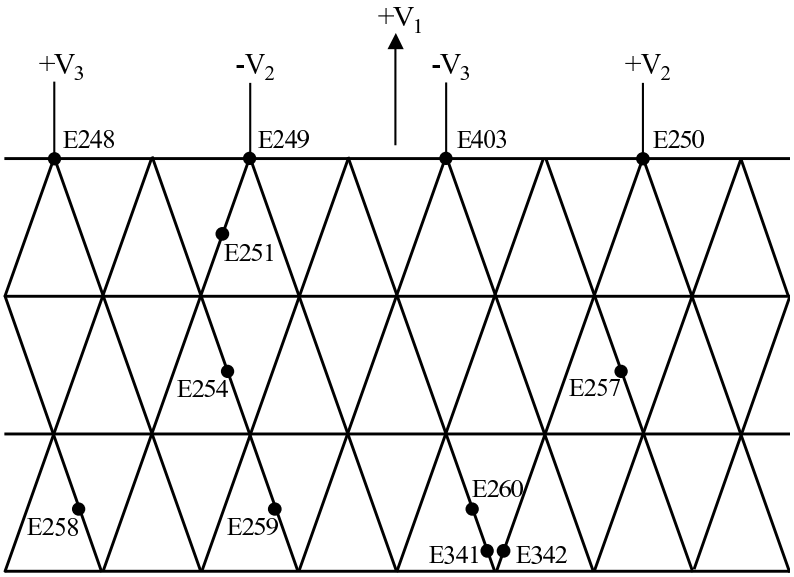

Fig. 16.— *Location of the thermal sensors along the MTS (drawn here as it was unfolded). We consider only the E248, E249, E250, E251, E254, E257, E258, E259, E260, E341, E342 and E403 thermistors. [Courtesy of Joshua Abel.]*

Along the Metering Truss Structure, which is a cylindrical truss that goes from station 257.5 to station 455.3 and that holds the primary and secondary mirrors in alignment, we consider 12 thermal sensors (E248, E249, E250, E251, E254, E257, E258, E259, E260, E341, E342 and E403), whose exact location is shown in Fig. 16. Using the readout values of these sensors, the Truss Axial Differential Temperature (T_{MTS-ax}) and the Truss Diametric Differential Temperature ($T_{MTS-dia}$) are defined as follows:

$$\begin{aligned} T_{MTS-ax} &= \frac{\mathrm{E258}+\mathrm{E259}+\mathrm{E260}+\mathrm{E341}+\mathrm{E342}}{5} - \frac{\mathrm{E248}+\mathrm{E249}+\mathrm{E250}+\mathrm{E403}}{4}; \\ T_{MTS-dia} &= \frac{\mathrm{E250}+\mathrm{E257}}{2} - \frac{\mathrm{E251}+\mathrm{E254}+\mathrm{E259}}{3}. \end{aligned}$$

For the Aft Shroud section of the spacecraft (that goes from station 100 to station 238) we consider 14 thermal sensors in total: 12 of them (T373, T374, T375, T376, T377, T378, T379, T380, T382, T384, T385 and T387) are located on the inner cylindrical section of the aft shroud, while 2 of them (T388 and T389) reside on the aft bulkhead outer surface as shown in Fig. 17. Using the readout values of these sensors, the Aft Shroud Temperature (T_{AS}) is defined as follows:

$$\begin{aligned} T_{AS} &= 0.115 \cdot (\mathrm{T388}+\mathrm{T389}) + 0.083 \cdot (\mathrm{T384}+\mathrm{T385}) + 0.064 \cdot (\mathrm{T373}+\mathrm{T374}+\mathrm{T375}+ \\ &+ \mathrm{T376}+\mathrm{T377}+\mathrm{T382}) + 0.062 \cdot (\mathrm{T378}+\mathrm{T379}) + 0.048 \cdot (\mathrm{T380}+\mathrm{T387}). \end{aligned}$$

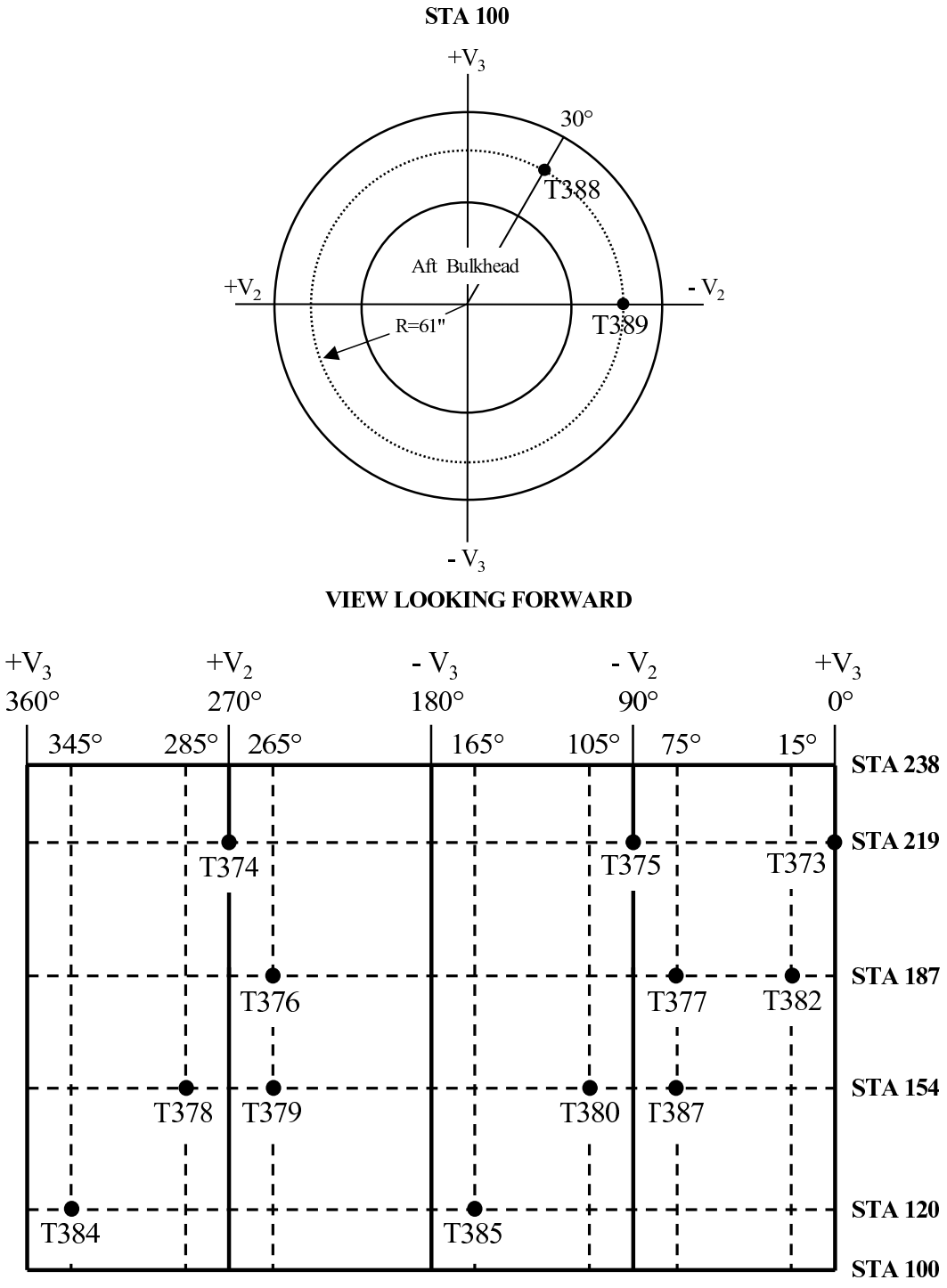

Fig. 17.— *Location of the Aft Shroud thermal sensors: T373, T374, T375, T376, T377, T378, T379, T380, T382, T384, T385, T387, T388 and T389 . Angles are measured from the $+V_3$ axis toward the $-V_2$ axis. Figure 2-27 from Yoshikawa, Castro & Piquero (1999).*